Observations of doubly excited states in lithiumlike calcium

J. Suleiman,* H. G. Berry, and R. W. Dunford
Physics Division, Argonne National Laboratory, Argonne, Illinois 60439

R. D. Deslattes
National Institute of Standards and Technology, Gaithersburg, Maryland 20899

P. Indelicato
Laboratoire de Physique Atomique et Nucléaire, Université Pierre et Marie Curie, 4 Place Jussieu, F-75252 Paris, France

(Received 15 July 1993)

We report observations of simultaneous electron excitation and electron capture in ion-atom collisions of 97-MeV Ca^{18+} and Ca^{19+} in an argon gas target. X-ray spectra at energies near 3.9 keV were collected using a high-resolution x-ray spectrometer. We have resolved transitions from doubly excited $1s2l2l'$ and $1s2l3l'$ states to singly excited $1s^22l'$ and $1s^23l'$ states in lithiumlike calcium. The observed transitions lie at energies close to the $1s2s$-$1s2p$ resonance transitions in heliumlike calcium. We compare the experimental wavelengths and intensities with relativistic Hartree-Fock calculations, and discuss the excitation mechanisms.

PACS number(s): 32.30.Rj, 34.50.Fa

I. INTRODUCTION

Ion-atom collision processes in which the transfer of a target electron to the projectile ion with simultaneous excitation of the projectile continue to be studied theoretically and experimentally to investigate the role of electron correlations in atomic collisions [1–7]. These studies are important because of the close relationship to dielectronic recombination (DR) which plays an important role in energy-transfer processes in astrophysical and laboratory plasmas. In particular, DR is an important energy-loss mechanism in magnetic fusion reactors. DR has been studied recently in electron-beam ion traps [8] (EBIT) and electron-beam ion sources [9] (EBIS), and in merged ion-electron beams [10].

Resonant transfer and excitation (RTE) occurs when projectile excitation and capture take place simultaneously in a single collision with the target atom through the electron-electron interaction between a projectile electron and a target electron, resonantly producing a doubly excited intermediate state. The resonant energies for such processes to doubly excited lithiumlike states are above 200 MeV for incident beams of hydrogenlike and heliumlike calcium. Hence, the cross sections we have observed at 100 MeV are dominated by the nonresonant transfer and excitation process (NTE). This is a process where two separate electron-nucleus interactions produce the intermediate state. In this paper, we present measurements of these processes where the fine structure of the excited states has been resolved. Hence, we are able to study the variation of the NTE cross section with the quantum numbers of these excited states.

We report here on observations of simultaneous electron excitation and capture in collisions of 97-MeV Ca^{19+} and Ca^{18+} ions on an argon gas target. X-ray spectra were collected near an energy of 3.9 keV using a high-resolution crystal spectrometer. This work was done as a part of precision measurements of the energies of the $n=1-2$ transitions in heliumlike calcium. However, measurements of the yield of doubly excited three-electron calcium ions from such collisions of both hydrogenlike and heliumlike calcium with the target have allowed the following:

(1) precision comparisons of experimental and theoretical transition energies (relativistic Hartree-Fock calculations);

(2) a beginning study of the collision mechanisms of simultaneous electron capture and excitation; and

(3) a better understanding of the satellite line structure near the resonance transitions of heliumlike calcium, which is important in precision wavelength determinations for these transitions.

II. EXPERIMENT

Calcium ions at 97 MeV were obtained using the acceleration-deceleration technique [11] at the ATLAS accelerator at Argonne National Laboratory. The ions were first accelerated to an energy of 200 MeV using a 9-MV tandem Van de Graaff accelerator, and the first half of a superconducting rf linear accelerator (LINAC). They were then stripped, mass selected, and decelerated in the final half of the rf LINAC to energies between 80 and 100 MeV. The target arrangement is shown in Fig. 1. The ion beam was focused through 1-mm apertures at either end of a 1-cm-long gas target, which was kept at a pressure of 10^{-1} torr. The beam current is measured in a

*Also at the Physics Department, University of Illinois, Chicago, IL 60680.

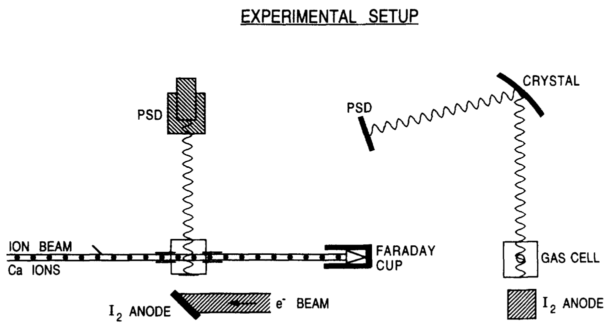

FIG. 1. The experimental setup, 97-MeV Ca^{18+} or Ca^{19+} projectiles into an argon gas target: a high-resolution crystal spectrometer views photons at 90° with respect to the beam. The spectrometer is equipped with a two-dimensional position-sensitive detector (PSD). An electron gun is used to provide calibration spectra.

shielded Faraday cup further down beam. The beam velocity was determined by measuring the time of flight of the projectiles to a precision of 1 part in 10^4.

The one-meter radius of curvature, curved crystal spectrometer views photons emitted approximately at right angles to the ion beam direction, and its dispersion is calibrated through observation of the iodine $L\alpha$ x-ray from an electron-irradiated target. The detector has two dimensions of spatial resolution. The dispersion direction is resolved through a wedge or "backgammon" plate anode following a proportional counter detector. A set of 12 wires provides a coarse resolution of about 1 mm in the perpendicular direction. Each wire spectrum can have a slightly different angular Doppler shift. The resulting twelve spectra are stored on line using the data acquisition by parallel and histogramming and networking (DAPHNE) [12] data collection system. They are analyzed separately in the subsequent data analysis. In the experiment, we obtained spectra for both hydrogenlike and heliumlike calcium beams incident on the target.

The calibration is in two parts: first the spectrometer is calibrated by use of the iodine $L\alpha$ x ray from the calibration source; second, the beam velocity is determined to high precision using the time-of-flight technique and used to make Doppler-shift corrections. Both parts are necessary to obtain absolute transition energies to precisions of a few parts in 10^5.

III. DATA ANALYSIS

The collision processes observed are the following:

(1) From the heliumlike beam,

(a) Single-electron capture and excitation,

$$Ca^{18+}+Ar\rightarrow Ca^{17+}(1s2l2l')\rightarrow Ca^{17+}(1s^2 2l')+(\text{x ray}), \tag{1}$$

$$Ca^{18+}+Ar\rightarrow Ca^{17+}(1s2l3l')\rightarrow Ca^{17+}(1s^2 3l')+(\text{x ray}) .$$

(b) Single-electron excitation (without capture),

$$Ca^{18+}+Ar\rightarrow Ca^{18+}(1s2p)+Ar\rightarrow Ca^{18+}(1s^2)+(\text{x ray}) . \tag{2}$$

(2) From the hydrogenlike beam:

(a) Single-electron capture,

$$Ca^{19+}+Ar\rightarrow Ca^{18+}(1s2p)+Ar^{1+}\rightarrow Ca^{18+}(1s^2)+(\text{x ray}) . \tag{3}$$

(b) Double-electron capture,

$$Ca^{19+}+Ar\rightarrow Ca^{17+}(1s2l2l')\rightarrow Ca^{17+}(1s^2 2l')+(\text{x ray}) , \tag{4}$$

$$Ca^{19+}+Ar\rightarrow Ca^{17+}(1s2l3l')\rightarrow Ca^{17+}(1s^2 3l')+(\text{x ray}) .$$

A spectrum obtained from collisions of heliumlike projectiles is shown in Fig. 2, and a spectrum obtained from collisions of hydrogenlike projectiles is shown in Fig. 3. The collision processes described by Eqs. (2) and (3) lead to emission of the heliumlike $1s^2$-$1s2p$ resonance lines, and are considered here only to calibrate accurately the observed doubly excited lithiumlike transitions arising from the processes of Eqs. (1) and (4).

In each experiment we collected 12 spectra corresponding to the 12 wires at the anode plane of the channelplate detector. In a preliminary analysis, the relative Doppler shifts of the 12 spectra were removed and the spectra summed.

We used the GRASP computer code [13–15] to make a Dirac-Hartree-Fock multiconfiguration calculation for the energies of some of the $1s2ln'l'$ doubly excited states, and their transition rates through electric dipole radiation to singly excited states. The states include all those of the $1s2l2l'$ and $1s2l3l'$ configurations and some states of $1s2l4l'$ configurations. The cases include $l=s,p$ and $l'=s,p,d$ electrons. In such a high nuclear charge ($Z=20$) system, spin-orbit mixing is strong, and almost

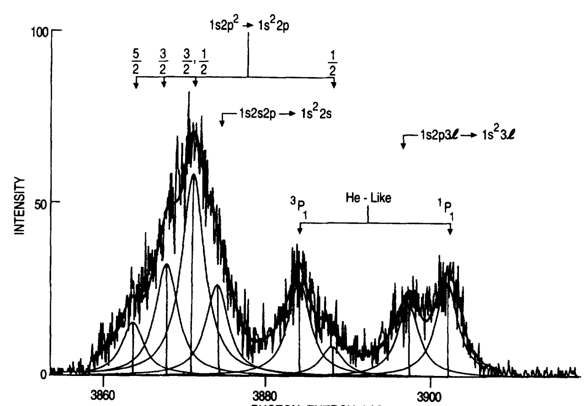

FIG. 2. Spectrum from the heliumlike beam, Ca^{18+}, on the argon gas target, producing an intermediate doubly excited Ca^{17+} which decays to singly excited states. The heliumlike transitions are also indicated in the spectrum. These He-like transitions are a result of one-electron excitation without capture.

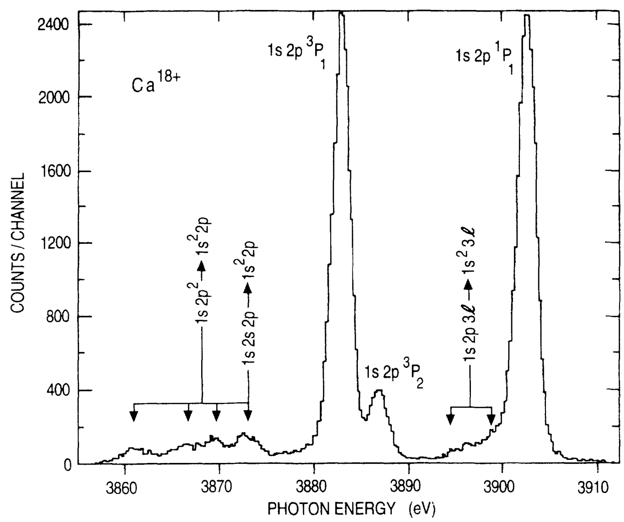

FIG. 3. Spectrum from the hydrogenlike beam, Ca^{19+}, on the argon gas target: one electron is captured producing the $1s2p$ excited state, which produces the strong decays from $^1P_1$, $^3P_1$, and $^3P_2$. The weak peaks are a result of double-electron-capture to the doubly excited lithiumlike states.

no eigenstates are pure *LS* or *JJ* coupled states. Hence, we obtain a large number of overlapping transitions.

A. Spectrum from the heliumlike incident beam

In order to compare our calculations from the GRASP code with the experimental data, we ordered the transitions by their transition probabilities (Einstein A coefficients) calculated from the GRASP code. We then retained only those transitions with $A \geq 10^{13}$ s^{-1}. All comparisons with observed spectra ignore the low probability transitions. We assume equal probability of populating each state within a given subsell. We can then proceed to the analysis of spectrum of Fig. 2, from the heliumlike beam. All such transitions within the observed spectral range are included in Tables I and II. We note that all such transitions calculated have lifetimes less than 10^{-12} s, so that all states decay in the field of view before leaving the gas cell. The widths of the lines were dominated by the Doppler spread due to the angular divergence of the beam.

Since the intensity $I \propto A/(n')^3$, we plotted the sum of this quantity using Gaussian line shapes, each Gaussian centered at its transition energy, and with a width taken from the fit to the spectrum; we also added to it the normalized intensities of the two heliumlike transitions, $1s2p\ ^1P_1 - 1s^2\ ^1S_0$ and $1s2p\ ^3P_1 - 1s^2\ ^1S_0$. Those intensities were first normalized by the intensity of the largest peak in the spectrum, then multiplied by the maximum of $\sum_{i=1}^{m} \{ A_i/(n_i')^3 \}$, where the sum is over all transitions calculated, see Fig. 4. This procedure allows an understanding of the theoretical spectrum. We notice that the first intense and broad peak obtained from our calculations (Fig. 4) has a shape very similar to the largest peak in the spectrum of Fig. 2. If we consider the other peaks from our calculations (e.g., $1s2l3l'$ to $1s^23l'$), we notice that their relative heights are different from the corresponding peaks in Fig. 2. This indicates that the different

TABLE I. Transition energies and decay rates for doubly excited states in lithiumlike calcium: comparisons between theory (the GRASP code) and experiment.

Initial State	Final State	Theory ΔE (eV) GRASP	Theory ΔE (eV) Desclaux	Experiment (eV)	Transition rate (10^{13} s^{-1})
$1s2p^2(^2D_{5/2})$	$1s^22p(^2P_{3/2})$	3863.34	3863.99	3862.15	8.03
$1s2p^2(^2P_{1/2})$	$1s^22p(^2P_{3/2})$	3865.63	3865.66	3866.82	6.6
$1s2p^2(^2D_{3/2})$	$1s^22p(^2P_{1/2})$	3867.28	3868.41		9.73
$1s2p^2(^2P_{3/2})$	$1s^22p(^2P_{3/2})$	3870.84	3871.01	3870.34	21.19
$1s2p^2(^2P_{1/2})$	$1s^22p(^2P_{1/2})$	3870.90	3870.72		17.90
$1s2s2p(^2P_{1/2})$	$1s^22s(^2S_{1/2})$	3872.21	3871.54		12.8
$1s2s2p(^2P_{3/2})$	$1s^22s(^2S_{1/2})$	3874.96	3874.38	3874.54	15.9
$1s2p^2(^2S_{1/2})$	$1s^22p(^2P_{3/2})$	3888.11	3889.17	3888.42	6.74
$1s2s2p(^2P_{1/2})$	$1s^22s(^2S_{1/2})$	3885.89			3.73
$1s2p3s(^2P_{3/2})$	$1s^23s(^2S_{1/2})$	3897.91		3897.62	13.6
$1s2p3s(^2P_{1/2})$	$1s^23s(^2S_{1/2})$	3898.45			13.3
$1s2p3d(^2D_{5/2})$	$1s^23d(^2D_{5/2})$	3899.11			12.4
$1s2p3d(^2D_{3/2})$	$1s^23d(^2D_{3/2})$	3899.19			15.2
$1s2p3d(^2D_{5/2})$	$1s^23d(^2D_{3/2})$	3899.58			3.89
$1s2p3p(^2D_{5/2})$	$1s^23p(^2P_{3/2})$	3896.75			13.9
$1s2p3p(^2P_{1/2})$	$1s^23p(^2P_{1/2})$	3897.96			13.8
$1s2p3p(^2D_{3/2})$	$1s^23p(^2P_{1/2})$	3897.88			13.50
$1s2p3p(^2P_{3/2})$	$1s^23p(^2P_{3/2})$	3898.44			14.8

TABLE II. Other possible transitions near 3902 eV with high transition rates.

Initial state	Final state	ΔE (eV) GRASP	Rate (10^{13} s^{-1})
$1s2p3d(^2F_{7/2})$	$1s^23d(^2D_{5/2})$	3901.03	13.1
$1s2p3d(^2F_{5/2})$	$1s^23d(^2D_{5/2})$	3902.23	3.1
$1s2p3p(^2S_{1/2})$	$1s^23p(^2P_{3/2})$	3903.68	9.8
$1s2p3d(^2F_{5/2})$	$1s^23d(^2D_{3/2})$	3902.69	9.8
$1s2p3d(^2P_{1/2})$	$1s^23d(^2D_{3/2})$	3904.66	15.3
$1s2p3d(^2P_{3/2})$	$1s^23d(^2D_{5/2})$	3905.27	13.9
$1s2p4s(^2P_{1/2})$	$1s^24s(^2S_{1/2})$	3900.63	16.6
$1s2p4s(^2P_{3/2})$	$1s^24s(^2S_{1/2})$	3900.84	16.4

subshells are not equally populated following the collision.

Cheng [16] has also calculated the Auger decay rates for doubly excited lithiumlike calcium. The results of this calculation show that inclusion of the Auger rates does not significantly change the relative yields. Figure 5 shows the expected yields, with and without the inclusion of the Auger rates. His radiative rates and transition energies agree well with those we have obtained using the GRASP code. One of us (Indelicato) [17] has calculated the transition energies independently, using the Desclaux relativistic Hartree-Fock code [18]. These results also agree well with those of the GRASP code; the results are given in Tables I and II.

Two groups of two of the transitions indicated in Tables I and II closely coincide in energy and are fitted as single lines. The limited spectral resolution and photon counting statistics of this spectrum allows us to fit just four lines to the initial strong and broad peak of the system.

The heliumlike transitions from $1s2p\ ^1P_1$ and $1s2p\ ^3P_{1,2}$ to the ground state $1s^2\ ^1S_0$ provide an accurate set of calibration lines, appearing partially blended in the spectrum of Fig. 2. The transition energies for those calibration lines are taken from calculations of Drake [19].

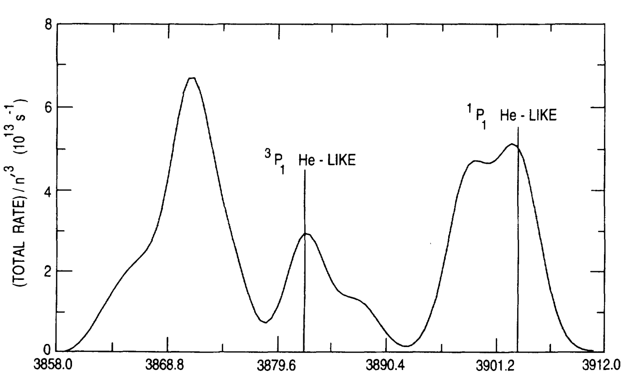

FIG. 4. The sum of all $A_i/(n_i')^3$ plotted in Gaussian shapes. The transitions include all $1s2l2l' \rightarrow 1s^22l'$, $1s2l3l' \rightarrow 1s^23l'$, and $1s2p4s \rightarrow 1s^24s$ plus the normalized intensity of the heliumlike transitions taken from the spectrum of Fig. 2.

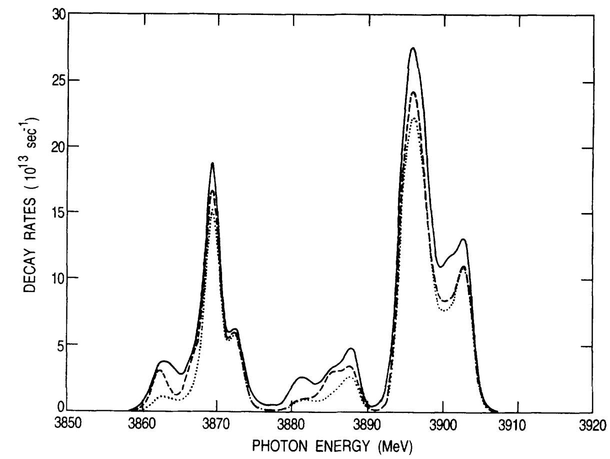

FIG. 5. Calculations by Cheng for the $1s2lnl$ doubly excited calcium states, where $n=2$ and 3. The solid curve is the sum of the radiative decay rates, the dashed curve includes radiative branching, and the dotted curve includes the radiative and Auger branching, all plotted in Gaussian shapes of 0.5-eV width. These results show that inclusion of the Auger rates does not significantly change the relative yields of these x-ray decays.

They are 3902.37 eV for the $^1P_1$-$^1S_0$ transition and 3883.31 eV for the $^3P_1$-$^1S_0$ transition.

B. Spectrum from the hydrogenlike incident beam

We point out that the heliumlike transitions appear more strongly in the spectrum of Fig. III. This occurs because the single-electron capture cross sections are much larger at these low velocities that the collisional excitation cross sections shown in Fig. 2.

The linewidths in the spectrum of Fig. 3 (2.35 eV) are much narrower than the linewidths in the spectrum of Fig. 2 (4.36 eV), because of the improved beam focusing conditions; the beam was focused to be parallel through the gas target, thus reducing the Doppler broadening of x rays emitted approximately perpendicular to the ion beam into the spectrometer. We were able to identify the first four peaks which appear in Fig. 3 between 3860 and 3877 eV as transitions of the type $1s^22p$-$1s2p^2$ and $1s^22s$-$1s2s2p$; these transitions are a result of double-electron capture. They appear weak compared to the heliumlike transitions from $1s2p\ ^1P_1$, $^3P_{1,2}$ in the same spectrum (Fig. 3). We note that the intensity ratios for the three transitions from the $1s2p^2$ levels remain the same, but the yield from the $1s2s2p$ level is enhanced for the hydrogenic incident beam.

The weighted averages for the transition energies obtained from these spectra are given in Tables I and II where they are compared with the GRASP calculations. We note that although the relative separations of the levels agree well with theory, the absolute theoretical energies are higher than experiment by approximately 2 eV. Higher-order nonrelativistic correlations may account for the difference.

IV. THE COLLISION MECHANISMS

In the collision with the incident heliumlike beam, we are observing transfer and excitation (TE), the transfer of one electron from the target to the projectile and at the same time the excitation of one of the projectile electrons. When the two electrons involved in the capture and excitation are correlated, the process is known as resonant transfer and excitation (RTE) and when the two electrons are uncorrelated the process is known as (NTE). Since the RTE resonance is near 200 MeV, the cross sections we have observed are dominated by NTE. Our measurements represent the first resolution of the excited-state fine structure during this process for three-electron ions, and can provide a good test of NTE calculations. No such calculations have yet been published. In our interpretation of the spectra, we have assumed equal probability of excitation (statistical) to the doubly excited states, so that the photon yields are proportional to the Einstein A coefficients.

Measurements of the double-electron-capture process in other ions have been made from ECR and EBIS sources at very low energies, e.g., see Refs. [20–22]. Most of these experiments measure the spectra of the autoionizing electrons at a fixed angle, but experiments measuring x rays have also been made [23]. Theoretical calculations have also been made for light target atoms [24,25]. Our measurements provide some high ion velocity measurements for the first time.

The double-electron-capture probability can be estimated roughly to be proportional to the product of two single-electron-capture probabilities, so we expect the double-electron-capture cross section to be small at such high energies compared to the single-electron-capture cross section. This explain why the intensity of the double-electron-capture peaks are weak compared to the intensity of the single-electron-capture peaks, both appearing in the spectrum of Fig. 3. The probability of creating these doubly excited states through two successive collisions is estimated to be much less at the low gas pressures used—it would involve two capture collisions, one of them including an excitation.

In the future, it would be interesting to vary the projectile energy, so that we can measure the energy dependence of the cross sections near the RTE resonance condition; in addition, lighter target such as helium or hydrogen would be used to enable better comparisons with theory. We plan to make such measurements using argon projectiles. Theoretical models of the expected populations for the two cases, resonant and nonresonant excitation, would be helpful, and especially to indicate where measurements would be most sensitive to testing the relative yields. The different angular-momentum states within a given subshell might be most sensitive. In addition, the faster decay might show effects of the receding fast ion as final-state interactions. Measurements of such processes would probably need measurements at even lower projectile energies.

ACKNOWLEDGMENTS

The authors thank K. T. Cheng of Lawrence Livermore Laboratory for helpful discussions and for providing us with the radiative and Auger transition rates for doubly excited lithiumlike calcium. This work was partially supported by the U.S. Department of Energy, Office of Basic Energy Sciences, under Contract No. W-31-109-ENG-38.

[1] D. Brandt, Phys. Rev. A **27**, 1314 (1983).
[2] J. A. Tanis *et al.*, Phys. Rev. Lett. **53**, 2551 (1984); J. A. Tanis, Phys. Rev. A **34**, 2543 (1986).
[3] D. H. Lee *et al.*, Phys. Rev. A **44**, 1636 (1991).
[4] Y. Hahan and H. Ramadan, Nucl. Instrum. Methods B **43**, 285 (1989).
[5] Philip L. Pepmiller, Patrick Richard, J. Newcomb, James Hall, and T. R. Dillingham, Phys. Rev. A **31**, 734 (1985).
[6] J. M. Feagin, J. S. Briggs, and T. M. Reeves, J. Phys. B **17**, 1057 (1984).
[7] W. G. Graham *et al.*, Phys. Rev. Lett. **65**, 2773 (1990).
[8] R. E. Marrs *et al.*, Phys. Rev. Lett. **60**, 1715 (1988).
[9] R. Ali *et al.*, Phys. Rev. Lett. **64**, 633 (1990).
[10] G. Kilgus *et al.*, Phys. Rev. Lett. **64**, 737 (1990); W. Spies *et al.*, Phys. Rev. Lett. **69**, 2768 (1992).
[11] R. W. Dunford, R. C. Pardo, M. L. A. Rapahelian, H. G. Berry, and R. D. Deslattes, Nucl. Instrum. Methods A **268**, 1 (1988).
[12] L. C. Welch, T. H. Moog, R. T. Daley, and F. Videbaek, IEEE Trans. Nucl. Sci. **NS-34**, 823 (1987).
[13] K. G. Dyall, Comput. Phys. Commun. **39**, 145 (1986).
[14] B. J. Mckenzie, I. P. Grant, and P. H. Norrington, Comput. Phys. Commun. **21**, 233 (1980).
[15] I. P. Grant, B. J. Mckenzie, P. H. Norrington, D. F. Mayers, and N. C. Pyper, Comput. Phys. Commun. **21**, 207 (1980).
[16] Private communication. We thank Dr. Cheng (Lawrence Livermore Laboratory) for allowing us to include his unpublished results in this paper.
[17] P. Indelicato, Nucl. Instrum. Methods **31**, 14 (1988).
[18] J. P. Desclaux, Comput. Phys. Commun. **9**, 31 (1975).
[19] G. W. Drake, Can. J. Phys. **66**, 586 (1988).
[20] M. Boudjema *et al.*, J. Phys. B **24**, 1713 (1991).
[21] P. Moretto-Cappelle *et al.*, J. Phys. B **22**, 271 (1989).
[22] M. Mack *et al.*, Phys. Rev. A **39**, 3846 (1989).
[23] A. Chetioui *et al.*, J. Phys. B **23**, 3659 (1990).
[24] Wolfgang Fritsch, Phys. Rev. A **45**, 6411 (1992).
[25] Ashok Jain and C. D. Lin, Phys. Rev. A **39**, 1741 (1989).